Ceramics International 44 (2018) 4961–4966

Contents lists available at ScienceDirect

Ceramics International

journal homepage: www.elsevier.com/locate/ceramint

Highly efficient $La_{0.8}Sr_{0.2}MnO_{3-\delta}$ - $Ce_{0.9}Gd_{0.1}O_{1.95}$ nanocomposite cathodes for solid oxide fuel cells

L. dos Santos-Gómez[a], J. Zamudio-García[a], J.M. Porras-Vázquez[a], E.R. Losilla[a], D. Marrero-López[b,*]

[a] Universidad de Málaga, Departamento de Química Inorgánica, Cristalografía y Mineralogía, 29071 Málaga, Spain
[b] Universidad de Málaga, Departamento de Física Aplicada I, Laboratorio de Materiales y Superficie, 29071 Málaga, Spain

ARTICLE INFO

Keywords:
Solid Oxide Fuel Cells
$La_{0.8}Sr_{0.2}MnO_{3-\delta}$
CeO_2
Spray-pyrolysis

ABSTRACT

$La_{0.8}Sr_{0.2}MnO_{3-\delta}$-$Ce_{0.9}Gd_{0.1}O_{1.95}$ (LSM-CGO) nanostructured cathodes are successfully prepared in a single process by a chemical spray-pyrolysis deposition method. The cathode is composed of nanometric particles of approximately 15 nm of diameter, providing high triple-phase boundary sites for the oxygen reduction reactions. A low polarization resistance of 0.046 Ω cm^2 is obtained at 700 °C, which is comparable to the most efficient cobaltite-based perovskite cathodes. A NiO-YSZ anode supported fuel cell with the nanostructured cathode generates a power output of 1.4 W cm^{-2} at 800 °C, significantly higher than 0.75 W cm^{-2} for a cell with conventional LSM-CGO cathode. The results suggest that this is a promising strategy to achieve high efficiency electrodes for Solid Oxide Fuel Cells in a single preparation step, simplifying notably the fabrication process compared to traditional methods.

1. Introduction

Solid Oxide Fuel Cells are considered as one of the most efficient electrochemical devices for electrical energy production; however, their commercialization is still hindered by the high operating temperatures and the premature degradation of the cell components [1–3]. In this context, the main research trend in SOFCs in last years is to reduce the operating temperature to the range of 600–800 °C.

The ohmic resistance of the conventional electrolyte, $Zr_{0.84}Y_{0.16}O_{1.92}$ (YSZ), has been significantly reduced by using thin film electrolytes [4]. Regarding the tradition cathode material, $La_{0.8}Sr_{0.2}MnO_{3-\delta}$ (LSM) is physically and chemically compatible with the YSZ electrolyte but exhibits poor catalytic activity for oxygen reduction reaction at temperatures below 800 °C. This is mainly related to its low ionic conductivity, which restricts the triple-phase boundary (TPB) sites, where the electrochemical reactions take place, near the electrolyte electrode-interface [5–7].

The addition of a second phase with high mixed ionic electronic conductivity to LSM is the main strategy to increase the TPB, and consequently, the cathode performance. Numerous studies have combined LSM with different ionic conductors, such as $Zr_{0.84}Y_{0.16}O_{1.92}$ (YSZ), $Ce_{0.8}Gd_{0.2}O_{1.9}$ (CGO) and $Bi_{1.5}Y_{0.5}O_{3-\delta}$ (BYO) [8–10]. The best results have been obtained by the addition of BYO due to the highest ionic conductivity and the fast oxygen incorporation in the lattice. However, the long term stability of this composite cathode is questionable because of the structural instability of Bi_2O_3-based electrolytes at intermediate temperatures [11]. Thus, LSM is usually combined with YSZ or CGO electrolytes.

The conventional composite cathodes are prepared by mechanically mixing the pristine materials, followed by sintering at high temperature onto the dense electrolyte. Unfortunately, it is difficult to control the composition distribution and architecture of the electrodes.

New microstructural designs and processing methodologies have been proposed in order enhance the electrocatalytic activity and durability of the cathodes. This includes, for example, electrode nanofibers and the infiltration/impregnation of an electrocatalytic active material into porous scaffold layers [12–20]. Most of these methods involve multiple preparation steps, and hence are unsuitable for industrial application. In addition, the high sintering temperatures needed to obtain an adequate adherence between the electrodes and the electrolytes, during the cell fabrication, leads to an excessive grain growth of the active material and the loss of performance [21]. In this context, spray-pyrolysis deposition is a simple and economic method to obtain films over large area at reduced temperature, which has been widely used to obtain different materials for SOFCs [22–25].

Recently, LSM-YSZ and LSM-BYO nanostructured powder cathodes have been obtained by co-sintering methods. It has been observed that the grain growth is limited during the sintering process due to the

* Corresponding author.
E-mail address: marrero@uma.es (D. Marrero-López).

https://doi.org/10.1016/j.ceramint.2017.12.089
Received 7 November 2017; Received in revised form 12 December 2017; Accepted 12 December 2017
Available online 15 December 2017

presence of the two phases, resulting in a mixture of nanometric particles with enhanced electrocatalytic activity and durability at intermediate temperatures [26,27].

In the present study, $La_{0.8}Sr_{0.2}MnO_{3-\delta}$ - $Ce_{0.9}Gd_{0.1}O_{1.95}$ (LSM-CGO) nanocomposite cathodes are prepared for the first time in a single step by a spray-pyrolysis deposition method, reducing the preparation time and costs compared to traditional methods. The nanostructured materials have been investigated by different structural, microstructural and electrical techniques, including X-ray diffraction, and scanning and transmission electron microscopy. Finally, the performance of the nanocomposite cathode is evaluated in anode supported SOFCs.

2. Experimental

50 wt% $La_{0.8}Sr_{0.2}MnO_{3-\delta}$ - $Ce_{0.9}Gd_{0.1}O_{1.95}$ (LSM-CGO) cathodes were deposited by chemical spray-pyrolysis. A precursor solution was obtained by dissolving in water stoichiometric quantities of $Ln(NO_3)_3{\cdot}6H_2O$ (Ln = La, Ce and Gd), $Sr(NO_3)_2$ and $Mn(NO_3)_2{\cdot}6H_2O$ (Sigma-Aldrich, purity above 99%). The solutions with concentration of 0.02 mol L^{-1} and flow rate of 20 mL min^{-1} were atomized in a spray nozzle, and deposited through a shadow mask of 0.3 cm^2 onto the substrates. Quartz plates were used as substrates for the structural analysis, and YSZ pellets and anode supported cells for the electrochemical characterization. The anode supported half cells, NiO(60 wt %)-YSZ(40 wt%)/YSZ, were fabricated following a procedure similar to that described elsewhere [28].

The spray-pyrolysis parameters: deposition temperature, time and nozzle-substrate distance were 250 °C, 1 h and 25 cm, respectively. Thereafter, the cells were treated in a furnace at 800 °C for 4 h in order to achieve crystallization of the cathode materials.

The structural analysis was performed by X-ray powder diffraction (XRD) with a PANalytical Empyrean diffractometer. The XRD patterns were analyzed by the Rietveld method using the GSAS program. During the analysis the usual parameters, such as scale factors, background and peak shape factors were refined, while the cation occupations were fixed to their stoichiometric values and not refined.

The morphology of the electrodes was examined by field emission scanning electron microscopy (FEI-SEM, Helios Nanolab 650) and high-angle annular dark-field scanning transmission electron microscopy (HAADF-STEM) (FEI, Talos F200X). Further experimental details can be found in [29,30].

The polarization resistance of the electrodes was determined by impedance spectroscopy in symmetrical cell configuration by using a frequency response analyzer (Solartron 1260 FRA) in the temperature range of 300–800 °C under open circuit voltage in air. Platinum ink and meshes were used as current collectors.

For the fuel cell tests, the single cells were sealed on an alumina tube support with a ceramic paste (Ceramabond 668, Aremco). The current–voltage and impedance plots were collected using a Bio-Logic VSP potentiostat/galvanostat/FRA at operating temperatures between 550 and 800 °C. Humidified H_2 (3 vol% water) and static air were used as fuel and oxidant, respectively. For the sake of comparison, a similar cell with conventional cathode was prepared and tested under identical conditions. For this purpose, 50 wt% CGO (Rhodia) and 50 wt% LSM (Praxair) powders were mixed in a ball-milling apparatus with zirconia vessel and balls at 100 rpm for 1 h, using Decoflux™ as organic vehicle. The resulting ink was screen-printed onto the electrolyte and sintered at 1100 °C for 1 h.

3. Results and discussion

3.1. Phase composition

The as-prepared LSM-CGO cathodes, deposited by spray pyrolysis at 250 °C, are amorphous and begin to crystallize above 650 °C (not shown). Since the operation temperature was limited at the intermediate temperature range, the cathodes are finally treated at 800 °C before further characterization.

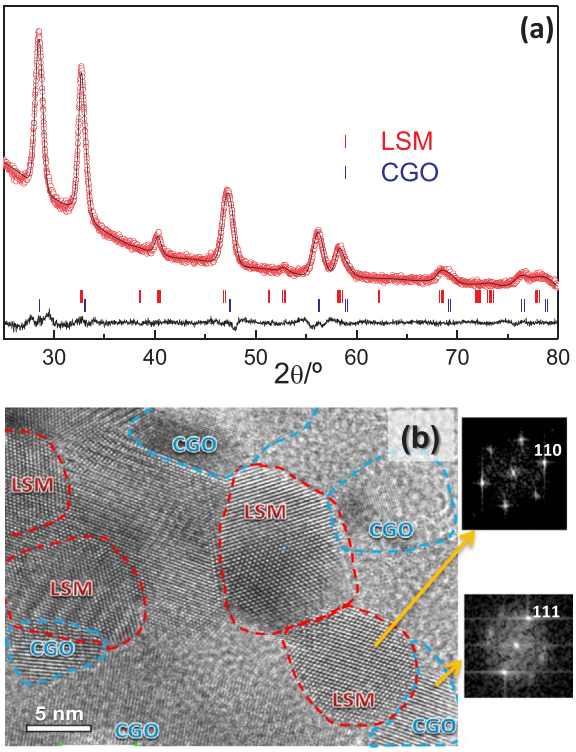

Fig. 1. (a) XRD pattern of the LSM-CGO nanocomposite cathode prepared by spray-pyrolysis deposition at 800 °C. (b) HRTEM image and electron diffraction patterns, showing nanometric particles of LSM and CGO.

Fig. 1a shows the XRD pattern of LSM-CGO deposited onto quartz plates. Two different crystalline phases, with perovskite and fluorite-type structures, are clearly identified. In addition, the position of the peaks matches well with the theoretical patterns of LSM and CGO (ICSD 51655 and 28796) [31]. Additional phases are not observed despite the co-sintering of LSM and CGO. Similar XRD patterns are obtained for the samples deposited on YSZ pellets.

XRD patterns were analyzed by the Rietveld method in the space groups $R\bar{3}c$ for LSM and $Fm\bar{3}m$ for CGO. The agreement factors were rather good, R_{wp} = 2.4% and R_F = 1.1% and 2.2% for CGO and LSM, respectively. The phase quantification was also in accordance with the nominal one: 52.2(1) wt% of LSM and 47.8(1) wt% of CGO. Regarding the unit cell volume, LSM exhibits a value of 351.48(21) Å3, which is somewhat lower than the bulk material, 351.8 $Å^3$ and can be explained by differences in oxygen stoichiometry and particle size effects [32]. In the case of CGO, the difference between the calculated and theoretical value is more important, 160.63(7) and 159.48 $Å^3$, respectively. This result indicates that CGO has a cation stoichiometry different from the proposed one, possibly due to minor cation incorporation of La3+ into the Ce4+ site with the consequent increase of the unit cell volume. It has to be commented that minor cation interdiffusion is not expected to negatively affect the electrical conductivity or electrocatalytic activity for the oxygen reduction [33].

The high-resolution transmission electron microscopy image (HTEM) analysis confirm that the composite cathode consists of a mixture of well crystallized particles, without the presence of amorphous domains after sintering at 800 °C (Fig. 1b). Moreover, the interatomic distances and selected area electron diffraction patterns for the different crystals are consistent with those reported for the bulk materials.

The microstructure of the cross-section of the cells was examined by SEM (Fig. 2a). The electrolyte is dense and has a thickness of about 6 μm. The electrodes exhibit excellent adhesion to the electrolyte and

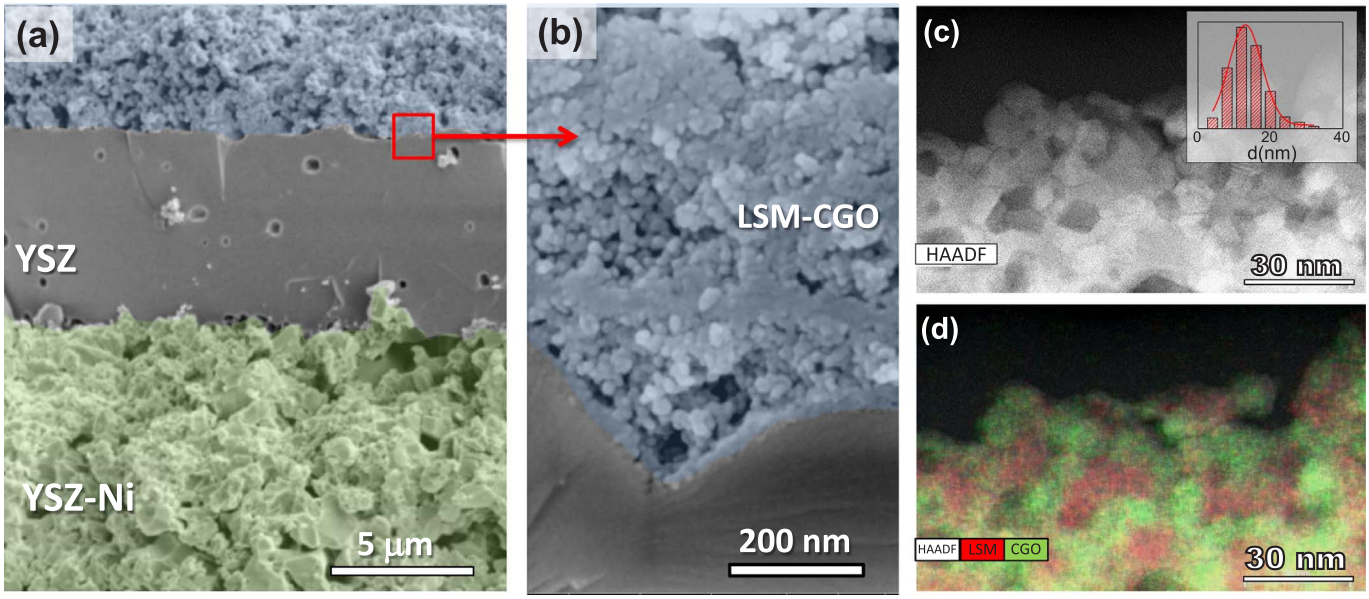

Fig. 2. (a) SEM image of the cross-section of the cells and (b) details of the cathode microstructure. (c) HAADF-STEM image and (d) EDS mapping of the nanocomposite cathode. The inset figure of (c) displays the grain size distribution.

high porosity for gas diffusion. The LSM-CGO cathode is formed by fine particles without appreciable morphological differences between the two compounds (Fig. 2b). In this case, the resolution of the FE-SEM instrument is not sufficient to distinguish between both phases by backscattering SEM and EDX.

HAADF-STEM image and EDX elemental mapping reveal an intimate mixture of LSM and CGO particles, ensuring proper ionic and electronic percolation paths, and therefore extended TPB sites for the ORR (Fig. 2c and d). The grain size, determined from the HAADF image, shows a typical Gaussian distribution with average grain size of 15.0 ± 4.5 nm (inset Fig. 2c).

Pure LSM cathodes were prepared in a previous work by spray-pyrolysis under similar synthetic conditions [34]. The most remarkable difference between pure and LSM-CGO cathodes is the average grain size, which decreases after the CGO addition, i.e. 50 nm for LSM and 15 nm for LSM-CGO. A small grain size of 50 nm is retained for LSM-CGO after sintering at 1000 °C for 2 h; however, under the same conditions, the blank LSM suffers a significant grain growth up to 200 nm as well as microstructure coarsening, which results in oxygen diffusion limitations, and consequently, poorer performance [34]. This behavior is explained by the presence of CGO as secondary phase, which limits the cation diffusion and the grain growth rate. A similar behavior was observed for related composite cathodes, such as LSCF-CGO and LSM-YSZ [26,35]. In comparison, the traditional LSM-CGO cathode sintered at 1100 °C for 1 h shows a particle size of approximately 300 nm, about 20 times larger than those of the nanocomposite.

3.2. Polarization resistance

The polarization resistance, R_p, of the cathodes was determined under symmetrical cell configuration by impedance spectroscopy. Since different contributions are involved in the polarization resistance, depending on the sample type, only the overall polarization resistance is determined and compared in Fig. 3. Note that the electrodes have been measured under identical experimental conditions for the sake of comparison.

The commercial LSM cathode with submicrometric particle size exhibits high values of polarization resistance at intermediate temperature, e.g. 3.5 Ω cm^2 at 700 °C. This value is drastically reduced for the traditional LSM-CGO cathode, 0.31 Ω cm^2 due to extended TPB length after CGO-addition. A similar value is obtained for the

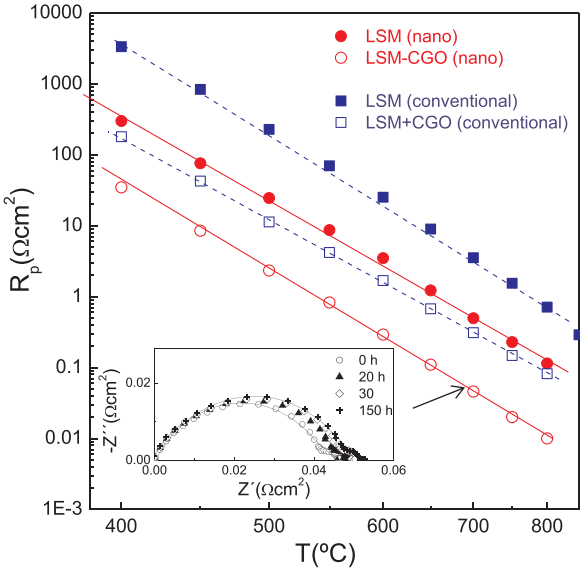

Fig. 3. Polarization resistance of different LSM-based cathodes with micrometric and nanometric grain size, obtained by screen-printing and spray-pyrolysis deposition, respectively. The inset figure shows the impedance spectra collected at 700 °C and different times.

nanostructured LSM cathode prepared by spray-pyrolysis, about 0.5 Ω cm^2. The lowest polarization resistances are obtained for the LSM-CGO nanocomposite cathode with values of only 0.045 and 0.01 Ω cm^2 at 700 and 800 °C, respectively. Thus, the polarization resistance of the nanostructured cathode, obtained by spray pyrolysis, is decreased by a factor of six compared to the conventional composite electrode. It has to be commented that these values of polarization resistance are, in general, lower than those previously reported in the literature for LSM – based cathodes with different compositions and microstructures (Table 1). For instance, 0.12 Ω cm^2 for LSM-CGO powder mixture [36], 0.05 Ω cm^2 for LSM-YSZ nanofibers [12], 0.27 Ω cm^2 for LSM-infiltrated YSZ nanofibers [13] and 0.05 Ω cm^2 for CSO-infiltrated LSM at a measured temperature of 800 °C [37]. Moreover, these R_p values are even comparable to those reported for cobaltite-based perovskite cathodes, i.e. 0.01 Ω cm^2 for

Table 1
Polarization resistance (R_p) at open-circuit voltage and maximum power density (P_{max}) for different LSM-based cathodes. Note that some data are given at different temperatures.

Composition	R_p (Ω cm^2) / T(°C)	P_{max} (W cm^{-2}) / T (°C)	[Refs.]
LSM (conventional)	0.72 / 800		This work
LSM-CGO (conventional)	0.08 / 800	0.75 / 800	This work
LSM-CGO (nano)	0.01 / 800	1.40 / 800	This work
LSM-YSZ (conventional)	0.06 / 800	1.00 / 800	[12]
LSM-YSZ (conventional)	1.00 / 800	–	[13]
LSM-CGO (conventional)	0.12 / 800	–	[35]
CSO-infiltrated LSM	0.05 / 800	1.16 / 800	[36]
LSM-YSZ (nanopowders)	–	2.65 / 800	[26]
LSM-$Bi_{1.6}Er_{0.4}O_3$ (nanopowders)	0.08 / 600	2.00 / 750	[27]
LSM-YSZ (nanofibers)	0.05 / 800	1.15 / 800	[12]
LSM-infiltrated YSZ (nanofibers)	0.27 / 800	–	[13]

$Ba_{0.5}Sr_{0.5}Co_{0.8}Fe_{0.2}O_{3-\delta}$ and 0.05 Ω cm^2 for nanostructured $Sm_{0.5}Sr_{0.5}CoO_{3-\delta}$ at 700 °C [38,39]. This performance improvement is clearly attributed to the fine microstructure of the LSM-CGO nanocomposite cathode with increased LSM/CGO interfaces for the oxygen reduction reactions.

A short stability test was carried out by annealing the nanocomposite cathode at 700 °C in air (inset Fig. 3a). The polarization resistance increased slightly for the first 30 h possibly due to minor microstructural changes, such as grain size growth. After that the values of resistance remained almost constant over time, confirming an excellent stability of the electrodes for applications at intermediate temperatures.

3.3. Single cell performance

The performance of the nanocomposite cathode is finally investigated under real SOFC conditions in anode supported cells with the following configuration: NiO-YSZ/YSZ/LSM-CGO. Fig. 4a and b compare the current-voltage (I-V) and current-power density (I-P) curves of two cells with traditional and nanocomposite cathodes, respectively, using humidified hydrogen as fuel and static air as oxidant. The OCV of both SOFCs is similar to the theoretical one, about 1.1 V, confirming excellent gas-tight sealing of the cell.

The cell with traditional cathode generates maximum power densities of 0.75 and 0.30 W cm^{-2} at 800 and 650 °C, respectively. In comparison, the cell with the nanocomposite cathode achieves higher power densities of 1.4 and 0.43 W cm^{-2} at 800 and 650 °C, respectively. Hence, the performance of this cell increases by a factor of 1.9 and 1.4 in the high and low temperature range, respectively. Table 1 compares the power density extracted from the literature for SOFCs with different LSM-based cathodes. The values vary in a wide range, depending on the cathode composition, microstructure and the electrolyte thickness, e.g. 1.0 W cm^{-2} for a commercial LSM-YSZ cathode [12], 1.15 W cm^2 for LSM-YSZ nanofibers [12], 1.16 W cm^2 at for CSO-infiltrated into LSM [37], 2.65 W cm^{-2} for LSM-YSZ nanocomposite powder cathode at 800 °C [26]; and 2 W cm^2 for LSM-$Bi_{0.6}Er_{0.4}O_3$ nanoparticles at 750 °C [27].

Fig. 4c shows representative impedance spectra at different temperatures for the cell with the nanocomposite cathode. The ohmic (R_s) and polarization resistances (R_p) are separated from the low and high

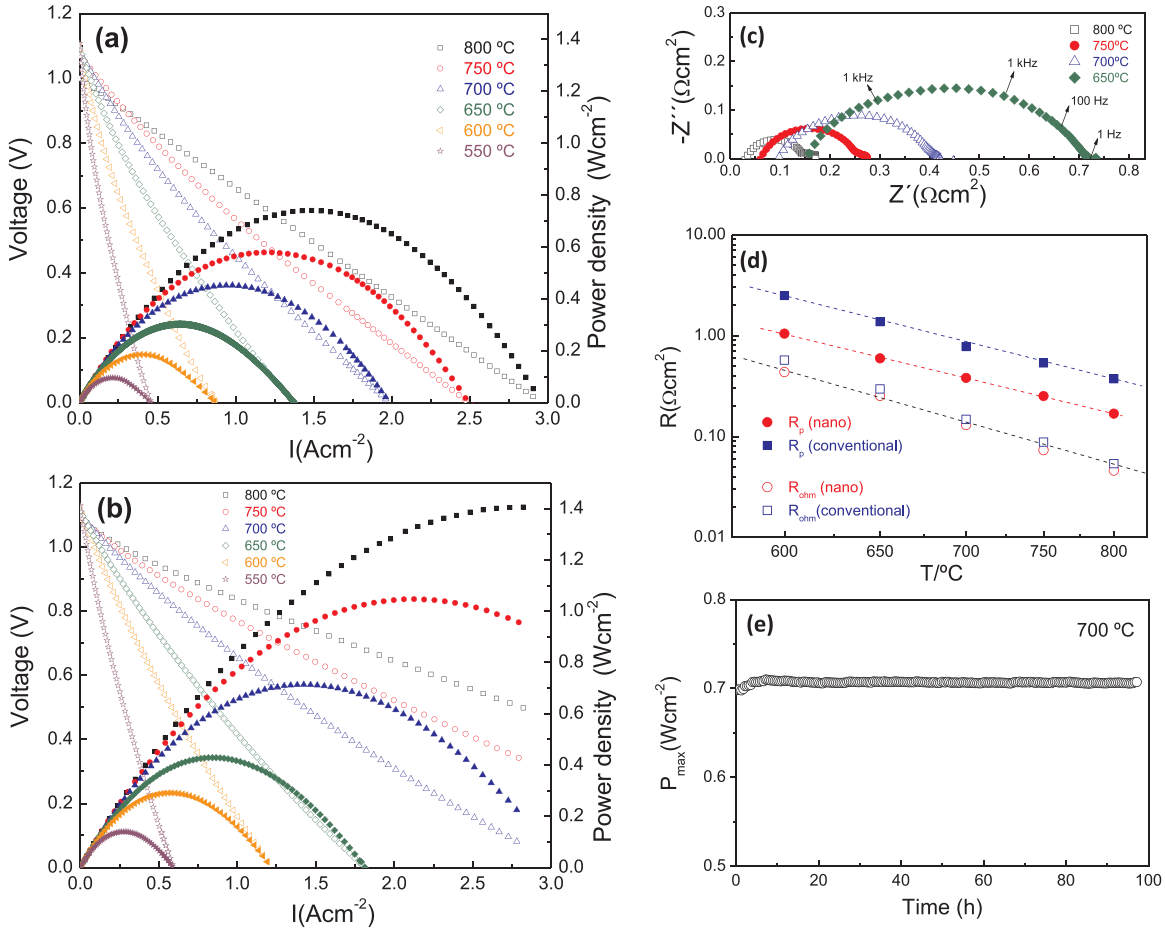

Fig. 4. Voltage and power density curves of NiO-YSZ/YSZ/LSM-CGO cells with (a) a traditional and (b) a nanocomposite cathode. (c) Impedance spectra acquired at different temperatures and (d) ohmic and polarization resistances for the cell with nanocomposite cathode at 0.5 V. (e) Variation of the power density over time at 700 °C.

frequency intercepts with the real axis (Fig. 4d). The ohmic resistance for both cells is practically identical because of the same anode/electrolyte microstructure. The cell with nanocomposite cathode exhibits lower overall polarization resistance (R_p); and as the YSZ electrolyte and Ni–YSZ anode are the same in both cells, the performance improvement is clearly related to cathode. Note also that R_p is higher than R_s for both SOFCs, indicating that the polarization contribution of the anode is significant, and hence, the performance might be improved by optimizing the anode microstructure.

After the I-V measurements, the durability of the cell was tested at 700 °C (Fig. 4e). After an initial improvement of the performance due to the current effect, which enhanced the catalytic activity of the electrodes, the power density shows no appreciable degradation [40]. Although the cathode is composed of very small particles, the cathode performance is maintained at 700 °C. Such high performance is associated with the highly dispersed LSM and CGO particles in the cathode, which prevent the grain growth during the SOFC fabrication and operation. These results demonstrate that LSM-CGO nanocomposites, prepared in a single process by spray pyrolysis, are potential cathode materials to operate efficiently at low temperature with performance comparable to cobaltite-based perovskite cathodes. A further interesting issue is that the nanocomposite cathodes are prepared in only one step, which is a clear advantage for industrial implementation.

4. Conclusions

Nanocomposite cathodes of LSM-CGO were prepared by using a single spray-pyrolysis deposition method from a precursor solution containing all cations in stoichiometric amounts. In this way, LSM and CGO were formed simultaneously, reducing drastically the preparation time, which is an important improvement for potential industrial application.

The CGO addition suppressed the grain growth of the nanocomposite cathodes, rendering lower particle size with respect to the blank LSM cathode, i.e. 15 nm for LSM-CGO and 50 nm for LSM after annealing at 800 °C. These differences were more important at high annealing temperatures, i.e. 50 and 200 nm at 1000 °C for LSM-CGO and LSM, respectively.

A single cell with LSM-CGO nanocomposite cathode generated a high power density of 1.4 W cm^{-2} at 800 °C, compared to 0.75 W cm^{-2} for a traditional cathode. Durability test of the cell over time showed a negligible degradation.

Acknowledgements

This work has been supported by EC2014-53906-R and MAT2016-77648-R and research grants (Spain). L. dos Santos-Gómez thanks to the Spanish Ministry of Education, Culture and Sports (FPU13/03030) for her FPU grant. J.M. Porras-Vázquez thanks the University of Málaga for the funding.

References

[1] E.D. Wachsman, K.T. Lee, Lowering the temperature of solid oxide fuel cells, Science 334 (2011) 935–939.
[2] Y. Zhang, R. Knibbe, J. Sunarso, Y. Zhong, W. Zhou, Z. Shao, Z. Zhu, Recent progress on advanced materials for solid-oxide fuel cells operating below 500 C, Adv. Mater. ⟨https://doi.org/10.1002/adma.201700132⟩.
[3] Z. Gao, L.V. Mogni, E.C. Miller, J.G. Railsback, S.A. Barnett, A perspective on low-temperature solid oxide fuel cells, Energy Environ. Sci. 9 (2016) 1602–1644.
[4] D. Beckel, A. Bieberle-Hütter, A. Harvey, A. Infortuna, U.P. Muecke, M. Prestat, J.L.M. Rupp, L.J. Gauckler, Thin films for micro solid oxide fuel cells, J. Power Sources 173 (2007) 325–345.
[5] S.P. Jiang, Development of lanthanum strontium manganite perovskite cathode materials of solid oxide fuel cells: a review, J. Mater. Sci. 43 (21) (2008) 6799–6833.
[6] C. Sun, R. Hui, J. Roller, Cathode materials for solid oxide fuel cells: a review, J. Solid State Electrochem. 14 (2010) 1125–1144.
[7] S.B. Adler, Factors governing oxygen reduction in solid oxide fuel cell cathodes, Chem. Soc. Rev. 104 (2004) 4791–4843.
[8] V. Dusastre, J.A. Kilner, Optimisation of composite cathodes for intermediate temperature SOFC applications, Solid State Ion. 126 (1999) 163–174.
[9] J.H. Choi, J.H. Jang, S.M. Oh, Microstructure and cathodic performance of $La_{0.9}Sr_{0.1}MnO_3$/yttria-stabilized zirconia composite electrodes, Electrochim. Acta 46 (2001) 867–874.
[10] L. Wu, Z. Jiang, S. Wang, C. Xia, (La,Sr)MnO_3–$(Y,Bi)_2O_3$ composite cathodes for intermediate-temperature solid oxide fuel cells, Int. J. Hydrog. Energy 38 (5) (2013) 2398–2406.
[11] S.E. Lin, W.C.J. Wei, Long-term degradation of Ta_2O_5-doped Bi_2O_3 system, J. Eur. Ceram. Soc. 31 (2011) 3081–3086.
[12] Y. Jeon, J.-H. Myung, S.-H. Hyun, Y.-G. Shul, J.T.S. Irvine, Corn-cob like nanofibres as cathode catalysts for an effective microstructure design in solid oxide fuel cells, J. Mater. Chem. A 5 (2017) 3966–3973.
[13] M. Zhi, N. Mariani, R. Gemmen, K. Gerdes, N. Wu, Nanofiber scaffold for cathode of solid oxide fuel cell, Energy Environ. Sci. 4 (2011) 417–420.
[14] N. Zhang, J. Li, Z. He, K. Sun, Preparation and characterization of nano-tube and nano-rod structured $La_{0.8}Sr_{0.2}MnO_{3-\delta}$/$Zr_{0.92}Y_{0.08}O_2$ composite cathodes for solid oxide fuel cells, Electrochem. Commun. 13 (2011) 570–573.
[15] L. Baqué, A. Caneiro, M.S. Moreno, A. Serquis, High performance nanostructured IT-SOFC cathodes prepared by novel chemical method, Electrochem. Commun. 10 (2008) 1905–1908.
[16] Z. Jiang, Z. Lei, B. Ding, C. Xia, F. Zhao, F. Chen, Electrochemical characteristics of solid oxide fuel cell cathodes prepared by infiltrating (La,Sr)MnO_3 nanoparticles into yttria-stabilized bismuth oxide backbones, Int. J. Hydrog. Energy 35 (2010) 8322–8330.
[17] D. Ding, X. Li, S. Lai, K. Gerdes, M. Liu, Enhancing SOFC cathode performance by surface modification through infiltration, Energy Environ. Sci. 7 (2014) 552–575.
[18] Z. Jiang, C. Xia, F. Chen, Nano-structured composite cathodes for intermediate-temperature solid oxide fuel cells via an infiltration/impregnation, Electrochim. Acta 55 (2010) 3595–3605.
[19] Z. Jiang, Z. Lei, B. Ding, C. Xia, F. Zhao, F. Chen, Electrochemical characteristics of solid oxide fuel cell cathodes prepared by infiltrating (La,Sr)MnO_3 nanoparticles into yttria-stabilized bismuth oxide backbones, Int. J. Hydrog. Energy 35 (2010) 8322–8330.
[20] L. Zhang, F. Zhao, R. Peng, C. Xia, Effect of firing temperature on the performance of LSM-SDC cathodes prepared with an ion-impregnation method, Solid State Ion. 179 (2008) 1553–1556.
[21] K. Chen, N. Ai, S.P. Jiang, Reasons for the high stability of nano-structured (La,Sr)MnO_3 infiltrated Y_2O_3-ZrO_2 composite oxygen electrodes of solid oxide electrolysis cells, Electrochem. Commun. 19 (2012) 119–122.
[22] A. Princivalle, D. Perednis, R. Neagu, E. Djurado, Porosity control of LSM/YSZ cathode coating deposited by electrospraying, Chem. Mater. 17 (2005) (1220-1127).
[23] X.-M. Wang, C.-X. Li, C.-J.G.-J. Yang, Microstructure and polarization of $La_{0.8}Sr_{0.2}MnO_3$ cathode deposited by alcohol solution precursor plasma spraying, Int. J. Hydrog. Energy 37 (2012) 12879–12885.
[24] L. dos Santos-Gómez, E.R. Losilla, F. Martín, J.R. Ramos-Barrado, D. Marrero-López, Novel microstructural strategies to enhance the electrochemical performance of $La_{0.8}Sr_{0.2}MnO_{3-\delta}$ cathodes, ACS Appl. Mater. Interfaces 7 (2015) 7197–7205.
[25] A. Princivalle, D. Perednis, R. Neagu, E. Djurado, Microstructural investigations of nanostructured La(Sr)$MnO_{3-\delta}$ films deposited by electrostatic spray deposition, Chem. Mater. 16 (2004) 3733–3739.
[26] H. Shimada, T. Yamaguchi, H. Sumi, K. Nomura, Y. Yamaguchi, Y. Fujishiro, Extremely fine structured cathode for solid oxide fuel cells using Sr-doped $LaMnO_3$ and Y_2O_3-stabilized ZrO_2 nano-composite powder synthesized by spray pyrolysis, J. Power Sources 341 (2017) 280–284.
[27] K.T. Lee, A.A. Lidie, H.S. Yoon, E.D. Wachsman, Rational design of lower-temperature solid oxide fuel cell cathodes via Nanotailoring of Co-assembled, Compos. Struct., Angew. Chem. Int. Ed. 53 (2014) 13463–13467.
[28] L. dos Santos-Gomez, J.M. Porras-Vazquez, E.R. Losilla, D. Marrero-López, Improving the efficiency of layered perovskite cathodes by microstructural optimization, J. Mater. Chem. A 5 (2017) 7896–7904.
[29] L. dos Santos-Gómez, J.M. Porras-Vázquez, F. Martín, J.R. Ramos-Barrado, E.R. Losilla, D. Marrero-López, An easy and innovative method based on spray-pyrolysis deposition to obtain high efficiency cathodes for Solid Oxide Fuel Cells, J. Power Sources 319 (2016) 48–55.
[30] D. Marrero-López, R. Romero, F. Martín, J.R. Ramos-Barrado, Effect of the deposition temperature on the electrochemical properties of $La_{0.6}Sr_{0.4}Co_{0.8}Fe_{0.2}O_{3-\delta}$ cathode prepared by conventional spray-pyrolysis, J. Power Sources 255 (2014) 308–317.
[31] Inorganic Crystal Structure Database, ICSD, 2017, pp. v2017-01.
[32] I. Fita, V. Markovich, A. Wisniewski, D. Mogilyansky, R. Puzniak, P. Iwanowski, L. Meshi, L. Titelman, V.N. Varyukhin, G. Gorodetsky, Size-dependent spin state and ferromagnetism in $La_{0.8}Ca_{0.2}CoO_3$ nanoparticles, J. Appl. Phys. 108 (2010) 063907.
[33] D. Pérez-Coll, D. Marrero-López, P. Núñez, S. Piñol, J.R. Frade, Grain boundary conductivity of $Ce_{0.8}Ln_{0.2}O_{2-\delta}$ ceramics (Ln=Y, La, Gd, Sm) with and without Co-doping, Electrochim. Acta 51 (28) (2006) 6463–6469.
[34] D. Marrero-López, L. dos Santos-Gómez, J. Canales-Vázquez, F. Martín, J.R. Ramos-Barrado, Stability and performance of nanostructured $La_{0.8}Sr_{0.2}MnO_3$ cathodes deposited by spray-pyrolysis, Electrochim. Acta 134 (2014) 159–166.
[35] Ö Çelikbilek, D. Jauffrès, E. Siebert, L. Dessemond, M. Burriel, C.L. Martin, E. Djurado, , Rational design of hierarchically nanostructured electrodes for solid oxide fuel cells, J. Power Sources 333 (2016) 72–82.
[36] A.J. Darbandi, T. Enz, H. Hahn, Synthesis and characterization of nanoparticulate films for intermediate temperature solid oxide fuel cells, Solid State Ion. 180 (2009)

424–430.
[37] D. Ding, M. Gong, C. Xu, N. Baxter, Y. Li, J. Zondlo, K. Gerdes, X. Liu, Electrochemical characteristics of samaria-doped ceria infiltrated strontium-doped $LaMnO_3$ cathodes with varied thickness for yttria-stabilized zirconia electrolytes, J. Power Sources 196 (2011) 2551–2557.
[38] Z. Shao, S. Haile, A high performance cathode for the next generation solid-oxide fuel cells, Nature 431 (2004) 170–173.
[39] L.M. Acuña, J. Peña-Martínez, D. Marrero-López, R.O. Fuentes, P. Nuñez, D.G. Lamas, Electrochemical performance of nanostructured $La_{0.6}Sr_{0.4}CoO_{3-\delta}$ and $Sm_{0.5}Sr_{0.5}CoO_{3-\delta}$ cathodes for IT-SOFCs, J. Power Sources 196 (2011) 9276–9283.
[40] D. Pérez-Coll, A. Aguadero, M.J. Escudero, L. Daza, Effect of DC current polarization on the electrochemical behaviour of $La_2NiO_{4+\delta}$ and $La_3Ni_2O_{7+\delta}$-based systems, J. Power Sources 192 (2009) 2–13.